Current Research in Food Science 10 (2025) 101103

Contents lists available at ScienceDirect

Current Research in Food Science

journal homepage: www.sciencedirect.com/journal/current-research-in-food-science

The effect of Gougunao tea polysaccharide on lipid metabolism in hyperlipidemia induced by a high-fat diet and its structural characteristics

Qihuan Deng [a,b,1], Shiyi Xiong [a,1], Wenjun Wang [a], Guodong Zheng [a], Jingjing Xie [a], Xiaojin He [a], Liang Ye [a], Lili Yu [a], Jingen Li [a,*]

[a] College of Food Science and Engineering, Jiangxi Agricultural University, Nanchang, 330045, China
[b] Citrus Research Institute, Southwest University, National Citrus Engineering and Technology Research Center, Chongqing, 400712, China

ARTICLE INFO

Handling Editor: Dr. Yeonhwa Park

Keywords:
Gougunao tea polysaccharide
Hyperlipidemia
Lipid metabolism
Structural characteristics

ABSTRACT

In this study, the effect of Gougunao tea polysaccharide (GTP40) on lipid metabolism in high-fat diet (HFD)-induced hyperlipidemic mice and its core structure were investigated. GTP40 effectively reversed the increase in weights of the liver and adipose tissues induced by HFD. The oxidative stress of the liver was also significantly alleviated following GTP40 intervention. According to the results of Real-Time quantitative Polymerase Chain Reaction (RT-qPCR), the genes associated with lipolysis were upregulated after GTP40 treatment, while lipogenesis-related genes were downregulated. Additionally, a homogeneous polysaccharide (GTP40–5P, obtained by degrading GTP40 for 5 h) with a molecular weight of 27858 Da was fractionated from GTP40 by the partial acid hydrolysis method. GTP40–5P was mainly composed of 62.30 ± 0.70 % neutral sugar, 54.82 ± 0.51 % uronic acid and 2.52 ± 0.74 % protein. The results of methylation and nuclear magnetic resonance (NMR) analysis indicated that the backbone of GTP40–5P was consisted of →4)-*α*-D-Gal*p*A-(1 → 4)-*β*-D-Gal*p*-(1→ units, with the terminal residue *β*-D-Gal*p*-(1→ linked to →3,4)-*α*-D-Gal*p*A-(1→ at the *O*-3 site, suggesting that it should be classified as homogalacturonan (HG)-type pectin with partial methyl esterification. These findings indicate that GTP40 alleviates lipid metabolism disorders in hyperlipidemic mice primarily *via* the AMPK signaling pathway. Furthermore, the elucidation of the primary structure of Gougunao tea polysaccharide enhances the understanding of the structure-activity relationship.

1. Introduction

Hyperlipidemia is a metabolic disease associated with lipid metabolic disorders. Excessive intake of a high-fat diet (HFD) is a key factor in inducing hyperlipidemia, and also serves as a risk factor for various diseases, such as obesity, type 2 diabetes mellitus (T2DM), metabolic dysfunction-associated steatotic liver disease (MASLD), hypertension, and cancers, which seriously affect health (Broadfield et al., 2021; Hegazy et al., 2020; Kang et al., 2023; Perez-Luz et al., 2023; Xu et al., 2024). AMP-activated protein kinase (AMPK) acts as an essential energy sensor widely distributed in diverse tissues and cells of human body and participates in the regulation of multiple of biological processes, including glucose metabolism, lipid metabolism, and protein metabolism (Heidary Moghaddam et al., 2022). Research findings have demonstrated that dysregulation of the AMPK pathway is closely related to the development and progression of numerous diseases, including hyperlipidemia (Bian et al., 2019). It has been reported that HFD can further lead to the accumulation of the white visceral adipose tissue and subcutaneous adipose tissue, along with significant up-regulation of several biomarker genes associated with adipogenesis and lipogenesis, such as peroxisome proliferator-activated receptor-γ (*PPAR-γ*), sterol regulatory element binding transcription factor-1c (*Srebp-1c*), acetyl-CoA carboxylase alpha (*ACCα*), and fatty acid synthase (*FAS*), which are critical targets for lipid metabolism disorder (Yuan et al., 2022).

Tea (Camellia sinensis) has gained popularity as an oriental leaf due to its numerous health benefits, and tea polysaccharides are receiving increasing attention because of their non-toxic nature and various biological activities, including antioxidation, antidiabetic effects, anti-hyperlipidemia, antitumor properties, anti-radiation capabilities, and et al. (Du et al., 2016). In our previous studies, a homogeneous fraction GTP40 was isolated from Gougunao tea, which alleviated HFD-induced

* Corresponding author. No. 1101, Zhimin Avenue, Economic and Technological Development Zone, Nanchang City, Jiangxi Province, China.
E-mail address: enen928@163.com (J. Li).
[1] These authors contributed equally to this work.

https://doi.org/10.1016/j.crfs.2025.101103
Received 1 March 2025; Received in revised form 28 May 2025; Accepted 30 May 2025
Available online 1 June 2025

hyperlipidemia by reducing oxidative stress and inflammatory responses, as well as restoring the balance of the gut microbiota (Deng et al., 2023). Nevertheless, the effect of GTP40 on fat accumulation and the regulation of lipid metabolism in hyperlipidemic mice remain unclear.

It is widely acknowledged that the structure of polysaccharides, including monosaccharide composition, molecular weight, glycosidic linkage type, residue sequence, the number and ratio of end groups, as well as the degree of substitution, plays a decisive role in their biological activities. To better understand the structure-function relationship of GTP40, its primary structure was investigated. However, the large molecular weight of complex polysaccharides often poses significant challenges for elucidating their primary structures (Gloaguen et al., 1997; Jin et al., 2012). Consequently, various depolymerization methods have been developed to reduce the molecular weight of polysaccharides, including acid hydrolysis (Pandeirada et al., 2022), oxidative degradation (Ma et al., 2021), enzymatic degradation (Xiong et al., 2019), as well as ultrasound and microwave degradation (Qiu et al., 2019). Among them, acid hydrolysis is a cost-effective and time-saving approach to degrade polysaccharides by selectively removing branches from the sugar chains while preserving the core structure characteristics. For instance, Rudtanatip et al. (2022) utilized trifluoroacetic acid (TFA) to degrade sulphated galactose (SG) isolated from *Gracilaria fisheri* and evaluated the antioxidant and protective effects of the low molecular weight SG (LMSG) against H_2O_2-induced oxidative stress in fibroblast cells. Their results demonstrated that LMSG showed greater antioxidant activity. Similarly, Duan et al. (2024) employed TFA to degrade *Belamcanda chinensis* (L.) DC. polysaccharides (BCP), thereby improving its water solubility and enhancing its anti-complement activity.

In this study, the effect of GTP40 on fat accumulation and the lipid metabolism regulation in hyperlipidemic mice induced by HFD, as well as its primary structure were investigated. The results not only deepen the understanding of the structure-activity relationship of GTP40, but also help open up a new path for the deep processing and application of Gougunao tea as a potential natural hypoglycemic agent.

2. Materials and methods

2.1. Materials

Gougunao tea was purchased from Tanghu Town, Suichuan County, Jiangxi Province of China. Trifluoroacetic acid (TFA) was purchased from Shanghai Aladdin Biochemical Technology Co., Ltd (Shanghai, China). The monosaccharide standards including *D*-fucose (Fuc), *L*-rhamnose (Rha), *L*-arabinose (Ara), *D*-mannose (Man), *D*-galactose (Gal), *D*-glucose (Glc), *L*-xylose (Xyl), *D*-fructose (Fru), *D*-ribose(Rib), *D*-galacturonic acid (GalA), *D*-glucuronic acid (GlcA), N-acetyl-*D*-glucosamine (GlcNAc), *D*-galactosamine hydrochloride (GalN), *D*-glucosamine hydrochloride (GlcN), *L*-guluronic acid (GulA), *D*-mannuronic acid (ManA) were from Bo Rui Saccharide Biotech Co., Ltd (Jiangsu, China). Dextran standards (M_w 1152, 5000, 11600, 23800, 48600, 80900, 148000, 273000, 409800, 667800 Da) were purchased from Sigma Chemical Co. Ltd (St. Louis, MO, USA). All other chemicals and solvents used were of analytical grade.

2.2. Extraction and partial acid hydrolysis of Gougunao tea polysaccharides

Based on our previous research (Deng et al., 2021), Gougunao tea was ground into fine powder using a high-speed pulverizer (Model DFY-500, Dade Chinese Traditional Medicine Machine Co., Ltd, Zhejiang, China), screened through a 40-mesh sieve, and then extracted with distilled water at 95 °C for 3.2 h with a solid-liquid ratio of 1:30 (g/mL) under the optimum extraction parameters. The extraction solution was filtered, concentrated, and then precipitated under gradient ethanol concentrations of 20 %, 40 %, 60 %, and 80 % (v/v), successively. GTP40 was obtained at an ethanol concentration of 40 % (v/v), with a high yield of 71.4 %.

According to the method of Kang et al. (2012), 2 g of GTP40 was hydrolyzed with 0.1 M TFA (10 mL) at 100 °C for 1 h, 3 h and 5 h, respectively. After hydrolysis, the samples were cooled to room temperature. After dialysis with distilled water (cutoff of M_w 8000–14000 Da), three volumes of anhydrous ethanol (v/v) were added for precipitation. The samples were stored at 4 °C overnight, and the precipitation was collected by centrifugation at 2683*g* for 15 min. The resulting products were named GTP40–1P, GTP40–3P, and GTP40–5P, corresponding to the hydrolysis times of 1, 3, and 5 h, respectively. The yield is calculated as the ratio of the dry mass of the sample before and after hydrolysis.

2.3. Animal experiment

Fifty male C57BL/6J mice (18 ± 2 g, 6 weeks old) were purchased from Hunan SJA Laboratory Animal Co., Ltd (Changsha, China) with the license number of SCXK (Xiang) 2019–0004. All mice were housed in a controlled environment (24 ± 2 °C, 50 ± 10 % relative humidity, 12 h light/12 h dark cycle) with free access to food and water. After a one-week acclimatization period, these mice were randomly divided into five groups (n = 10). One group was fed with a normal diet (ND group), while the other groups were fed with high-fat diet (HFD group). After 7 weeks of HFD feeding, the four HFD groups were administrated with 10 mg kg^{-1} simvastatin (SIM group), 400 mg kg^{-1} of GTP40 (GTP40-L group), 800 mg kg^{-1} of GTP40 (GTP40-H group) and physiological saline (HFD group) *via* daily oral gavage once a day for another 8 weeks, respectively. The high-fat diet (H10060, 60 % of energy from fat) and the normal diet (H10010, 10 % of energy from fat) were purchased from Beijing Huafukang Biotechnology Co., Ltd., and their composition were detailed in Table S1. Body weight was recorded weekly. All experimental procedures involving animals were conducted in accordance with the guidelines of the National Research Council's Guide for the Care and Use of Laboratory Animals, and the Chinese Society for Laboratory Animals, and were approved by the Animal Care and Use Committee of Jiangxi Agricultural University (No. 2022–001).

At the end of the experiment, the mice were fasted overnight with free access to water and then anesthetized with diethyl ether. Blood was collected by eyeball extirpation, followed by centrifugation at 724*g* for 15 min at 4 °C. The serum was immediately snap-frozen in liquid nitrogen and then stored at −80 °C. Subsequently, the mice were euthanized by cervical dislocation, and the liver and adipose tissues (perirenal white adipose tissues, pWAT; epididymal white adipose tissues, eWAT; subcutaneous inguinal white adipose tissues, sWAT; and brown adipose tissue, BAT) were collected and weighted, these adipose tissue and liver indices were calculated based on the ratio of tissue weight to body weight. A portion of the adipose tissue was fixed with 4 % paraformaldehyde, while the remaining portion was stored at −80 °C for further analysis.

2.4. Liver biochemical analysis

The activities of superoxide dismutase (SOD), malondialdehyde (MDA), glutathione peroxide (GSH-Px), alanine aminotransferase (ALT), and aspartate transaminase (AST) in the liver were assayed using commercial kits (Nanjing Jiancheng Bioengineering Institute, Nanjing, China) according to the manufacturer's instructions.

2.5. Histological analysis of adipose tissues

The fixed adipose tissues were meticulously trimmed, dehydrated, embedded, sliced, stained, and sealed according to the procedure of pathological experimental examination. All the stained samples were examined under an optical microscope (Nikon Eclipse E100, Nikon, Japan).

2.6. RT-qPCR analysis

Total RNA extraction from the liver, sWAT and BAT tissues, reverse transcription, and RT-qPCR were performed as previously described (Zhang et al., 2024). The mRNA expression levels of FAS, UCP1, ACCα, AMPK-α, SREBP-1c, Adipor1, CPT-1α, and PPARα were quantified using the $2^{-\Delta\Delta Ct}$ method. The primers were synthesized by Beijing Genomics Institute, and the primer sequences were listed in Table S2.

2.7. Chemical composition analysis

The contents of neutral sugars, proteins, and glucuronic acid of GTP40–1P, GTP40–3P, and GTP40–5P were determined by phenol-sulfuric acid method (Chen et al., 2023), Coomassie brilliant blue method (Bradford, 1976), and *m*-hydroxybiphenyl method (Qiu et al., 2022), using D-glucose, bovine serum albumin, and D-galacturonic acid as standards, respectively.

2.8. Determination of the molecular weight and monosaccharide composition

The molecular weight and monosaccharide composition of GTP40–5P were determined according to our previously reported method (Dong et al., 2024). The molecular weight was measured by a Shimadzu LC-10A high performance gel permeation chromatography (HPGPC) system (Tokyo, Japan), while the monosaccharide composition was analyzed by a high-performance anion exchange chromatography (HPAEC) system (Thermo Fisher Scientific Inc., US) equipped with a pulsed amperometric detector (PAD).

2.9. Methylation analysis

The linkage types of sugar residues were determined by the methylation experiment. The partially methylated alditol acetates (PMAAs) derived from GTP40–5P were prepared strictly according to the method described in our previous study (Li et al., 2020). The PMAA solution was analyzed using a gas chromatography-mass spectrometry (GC-MS) system (Shimadzu GCMS-QP2010, Japan) equipped with an RXI-5 SIL MS capillary column (30 m × 0.25 mm, 0.25 μm film thickness, Shimadzu, Japan). The temperature program was set as 120–250 °C at 3 °C/min, maintaining at 250 °C for 5 min. The inlet temperature was 250 °C, the detector temperature was 250 °C, the carrier gas was helium, and the flow rate was 1 mL/min.

2.10. NMR spectroscopy analysis

50 mg of GTP40–5P was dissolved in 0.5 mL of deuterium oxide (D_2O, 99.9 %) and freeze-dried. The dried samples were redissolved in 0.5 mL of D_2O and freeze-dried again. This operation was repeated at least three times until all the hydrogen (H) was substituted by deuterium (D). For the final time, the samples were dissolved in D_2O again and stirred at room temperature for 3 h before NMR analysis. The 1D/2D NMR spectra of hydrogen spectrum (^1H), carbon spectrum (^{13}C), correlation spectrum (COSY), heteronuclear single quantum coherence (HSQC), nuclear overhauser effect spectrum (NOESY), and heteronuclear multiple bond correlation (HMBC) were measured by a 600 MHz Bruker spectrometer (Bruker, Germany) at 25 °C. Deuterated acetone was used as an internal standard.

2.11. Statistical analysis

Data were presented as mean ± standard deviation (m ± SD). Statistical significance was determined using one-way analysis of variance (ANOVA) and the LSD test to compare the differences among different groups by IBM SPSS Statistics 25.0. $p < 0.05$ indicated statistical significance.

3. Results and discussion

3.1. Effect of GTP40 on the liver biochemical indices

It is widely acknowledged that the liver is an active organ for lipid oxidation, and stimulating lipid metabolism may help inhibit the accumulation of hepatic and visceral fat (Chao and Huang, 2020). SOD and GSH-Px are antioxidase, while MDA is a product of lipid peroxidation (Kim et al., 2017). These indicators can reflect the extent of oxidative damage. As presented in Fig. 1, 15 weeks of HFD feeding significantly increased the body weight in the HFD group compared with the ND group ($p < 0.05$). The liver index has no significant difference between ND group and HFD group ($p > 0.05$). However, the body weight was significantly reduced in both the SIM and GTP40 groups compared with the HFD group ($p < 0.05$). Additionally, after 8 weeks of GTP40 treatment, SOD, AST, and GSH-Px activities in the liver increased significantly compared with those in the HFD group ($p < 0.05$), whereas MDA levels in the liver were significantly decreased ($p < 0.05$). These effects were similar to those observed in the SIM group. However, there were no significant differences in ALT levels among these groups ($p > 0.05$). These results indicated that GTP40 could improve oxidative stability, decrease lipid peroxidation and protect the liver.

3.2. Lipid accumulation of different adipocytes

Adipose tissue is classified into white adipose tissue (WAT) and brown adipose tissue (BAT) (Hung et al., 2014). WAT, the primary site of energy storage, undergoes an increase in adipocyte size and a relatively high organ weight in obesity (Wang et al., 2018). BAT is a natural energy-consuming adipocyte tissue with a large quantity of mitochondria and multi-chamber lipid droplets, being capable of generating heat rather than energy. As presented in Fig. 2A–E, the adipose tissue indices of eWAT, sWAT, and pWAT were significantly higher in the HFD group compared with the ND group, while BAT index was significantly reduced ($p < 0.05$). However, after the 8-week intervention of GTP40, the adipose tissue indices of eWAT, sWAT, and pWAT were significantly decreased in both the GTP40-L and GTP40-H groups ($p < 0.05$), while the BAT index was significantly increased ($p < 0.05$), approaching levels comparable to those in the ND group. Additionally, the SIM group also exhibited a significant inhibitory effect on the adipose tissue indices of sWAT and pWAT ($p < 0.05$), along with an increase in the index of BAT ($p < 0.05$).

To evaluate the histological changes of adipose tissues in hyperlipidemic mice, eWAT, sWAT, pWAT, and BAT were stained by hematoxylin-eosin (H&E) staining. Compared with the ND group, the HFD group showed significantly enlarged fat cell size, irregular morphology, and decreased fat cell number under the same field of vision (Fig. 2F–J). The results of the SIM group were not significantly different from those of the HFD group ($p > 0.05$). Notably, both GTP40-L and GTP40-H interventions significantly reduced the adipocyte area compared with the HFD group ($p < 0.05$), particularly in the GTP40-H group. It implied that GTP40 effectively reduced adipose accumulation in HFD-induced hyperlipidemic mice.

3.3. Effect of GTP40 on the expression of genes associated with lipid metabolism in the liver and adipose tissue

To investigate the potential molecular mechanism of GTP40 in ameliorating the lipid metabolism disorders in hyperlipidemic mice fed with HFD, the expression levels of several representative lipid metabolism-related genes in the liver and adipose tissue were investigated. *Adipor1* is an upstream regulator of AMP-activated protein kinase (*AMPK*) that promotes its activation (Okada-Iwabu et al., 2013). The phosphorylation of *AMPK* reduces triglyceride (TG) levels by inhibiting the expression of sterol regulatory element-binding protein-1c (*SREBP-1c*) and indirectly decreasing the expressions of its downstream

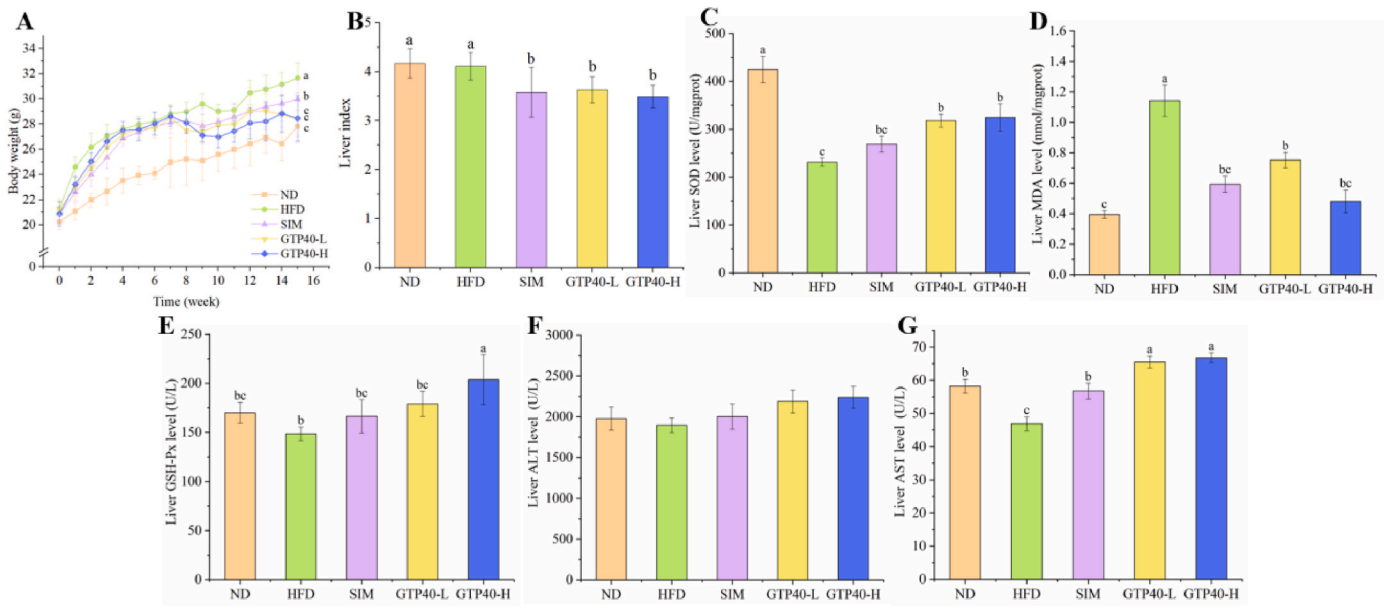

Fig. 1. Influence of GTP40 on the body weight, antioxidant indices and lipid levels in liver. (A) Body weight, (B) Liver index, (C) SOD, (D) MDA, (E) GSH-Px, (F) ALT, and (G) AST levels in liver. Values were expressed as m ± SD (n = 6). Data with different letters varied significantly ($p < 0.05$). SOD, superoxide dismutase; MDA, malondialdehyde; GSH-Px, glutathione peroxide; ALT, alanine aminotransferase; AST, aspartate transaminase.

targets, fatty acid synthase (*FAS*) and acetyl-CoA carboxylase *α* (*ACCα*) (Han et al., 2019). Additionally, *AMPK* phosphorylation stimulates the expression of proliferator-activated receptor *α* (*PPARα*), which regulates lipid metabolism through the modulation of the downstream factor of carnitine palmitoyltransferase-1*α* (*CPT-1α*). *CPT-1α* promotes the transport of fatty acids (FA) into mitochondria for *β*-oxidation (Fan et al., 2022).

The RT-qPCR results (Fig. 3A–G) indicated that, with the intervention of GTP40, the mRNA expressions of *Adipor1*, *AMPK-α*, *PPARα*, and *CPT1α* were significantly upregulated compared with the HFD group ($p < 0.05$), whereas the mRNA expressions of *SREBP-1c*, *FAS*, and *ACCα* were significantly downregulated ($p < 0.05$). The trend was consistent with the SIM group. Moreover, the activation of *AMPK* increases lipolysis metabolism and reduces the expression levels of lipid synthesis-related factors such as *SREBP-1c*, *FAS*, *ACCα*, thereby decreasing lipid accumulation, consistent with the findings of Pan et al. (2018). BAT burns glucose and fatty acids through the action of uncoupling protein 1 (*UCP1*), which decouples substrate oxidation from ATP production (Auclair et al., 2020). *UCP1* plays a critical role in energy dissipation through non-shivering thermogenesis in thermogenic adipocytes (Lu et al., 2016). Accumulating evidence implies that activating the activity of BAT has emerged as an attractive approach for increasing energy expenditure in metabolic diseases induced by HFD (Ju et al., 2019; Karise et al., 2019). As shown in Fig. 3H–I, GTP40 administration produced effects comparable to those observed in the SIM group, with both significantly increasing *UCP1* expression in sWAT and BAT ($p < 0.05$).

In conclusion, GTP40 exhibits a significant regulatory effect on lipid metabolism in hyperlipidemic mice. However, since this study did not assess water intake, food intake, and energy expenditure, further research is essential to comprehensively elucidate is underlying mechanism. Current evidence suggests that most polysaccharide treatments do not significantly affect food intake in HFD-fed mice (Yuan et al., 2022; Zhu et al., 2018). Nevertheless, several studies have shown that polysaccharides can enhance butyric acid production by modulating the gut microbiota (Lan et al., 2022; Yang et al., 2021). By promoting glucagon-like peptide-1 (GLP-1) secretion and BAT activation, butyrate helps maintain satiety and prevents HFD-induced weight gain (Li et al., 2018). Therefore, further investigation is warranted to examine the effects of GTP40 on appetite regulation and intestinal flora composition, clarifying its regulatory mechanism on lipid metabolism from the perspective of the gut-brain axis. Additionally, as no similar fiber control was included in this study, it remains unclear whether the observed effects are specific to GTP40 or represent a general effect comparable to those of other types of fibers.

3.4. The yields, molecular weights, and monosaccharide compositions

The results were summarized in Table 1. The yields of three hydrolyzates (GTP40–1P, GTP40–3P, and GTP40–5P) were approximately 26 %, 25 %, and 18 %, respectively. M_w and M_n were calculated according to the regression equation of $\log M_w = -0.1889x+12.007$ ($R^2 = 0.9943$) and $\log M_n = -0.1752x+11.304$ ($R^2 = 0.9931$), where x represented the retention time. The polymer dispersity index (PDI, M_w/M_n) of GTP40–1P, GTP40–3P and GTP40–5P were 1.599, 1.545 and 1.427, respectively, indicating that GTP40–5P had the narrowest molecular weight distribution (Fig. 4A). Therefore, GTP40–5P was selected for the subsequent structural analysis experiments. The monosaccharide composition of GTP40–5P was presented in Fig. 4C. The results indicated that GPT40–5P was composed of Rha, Gal, Glc, Xyl, Man and GalA with a molar percentage of 1.5:9.7:1.3:0.7:0.7:86.1. Thus, GTP40–5P was presumed to be mainly composed of GalA, which might possess a homogalacturonan (HG) structure.

3.5. Structure characteristics of GTP40–5P

3.5.1. Methylation analysis

Methylation analysis is a classical method to determine the types of glycosidic bond of polysaccharides (Yang et al., 2022). Since all the galacturonic acid residues were reduced to galactose before methylation, no galacturonic acid residue could be detected. As presented in Table 2 and Fig. 5, three types of galactose residues were identified. *t*-Gal*p*1→ was the only terminal residue (7.6 %), →3,4-Gal*p*1→ was the branching sugar residue (12.34 %), and →4-Gal*p*1→ was the unsubstituted residue (80.06 %). Combined with the results of monosaccharide composition, GTP40–5P was presumably composed of →4-Gal*p*A1→ as the backbone, with branches at *O*-3 terminated by *t*-Gal*p*A or *t*-Gal*p*.

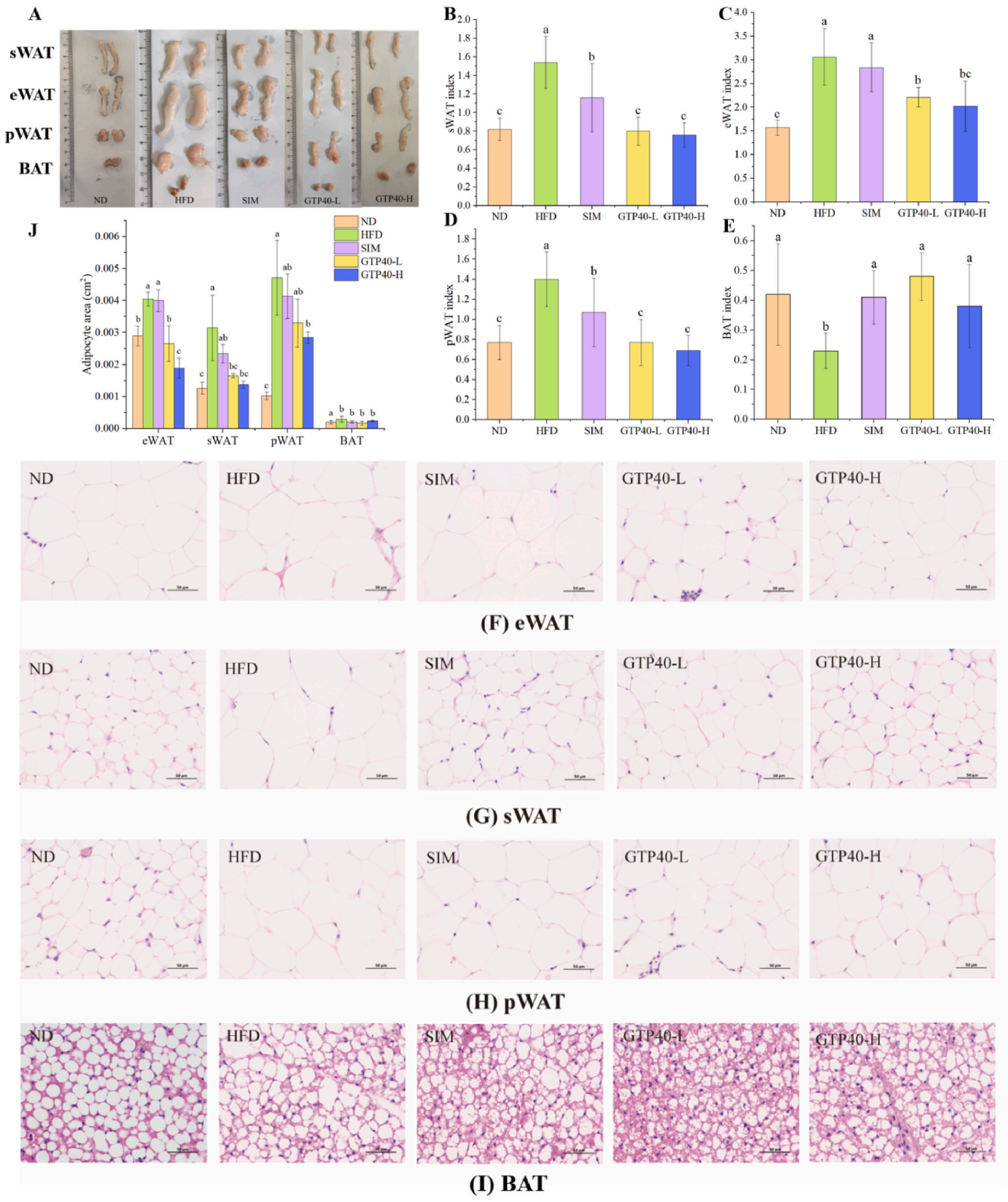

Fig. 2. Changes in adipocyte tissue of mice in different groups during the experimental period. (A) The appearance of four types of adipose tissue; Indices of (B) eWAT, (C) sWAT, (D) pWAT, and (E) BAT; H&E staining of (F) eWAT, (G) sWAT, (H) pWAT, and (I) BAT at 200 × of magnification, and fat cells area of (J) eWAT, sWAT, pWAT, and BAT. Values were expressed as m ± SD (n = 5). Data with different letters varied significantly ($p < 0.05$). pWAT, perirenal white adipose tissues; eWAT, epididymal white adipose tissues; sWAT, subcutaneous inguinal white adipose tissues; BAT, brown adipose tissue; H&E staining, hematoxylin-eosin staining.

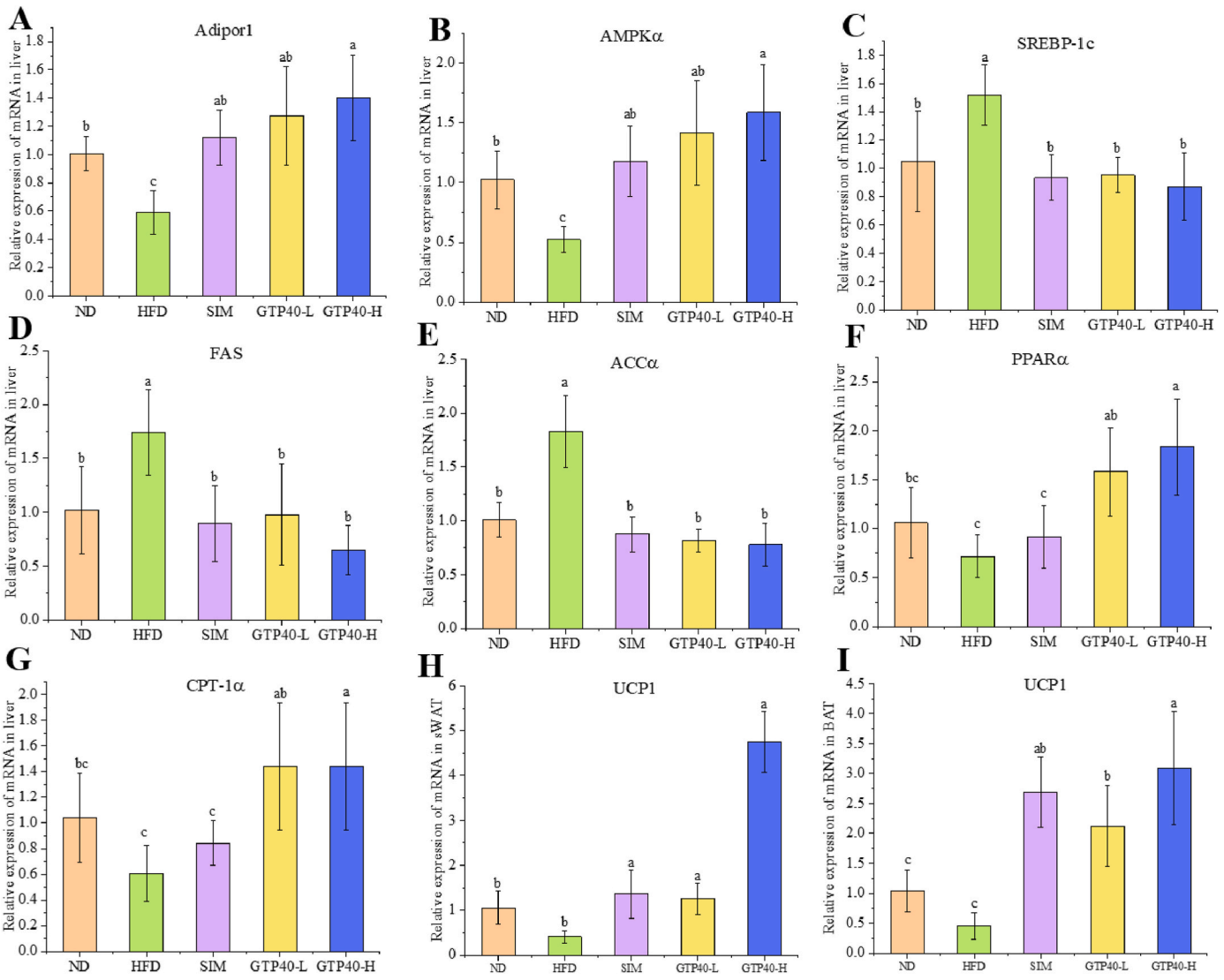

Fig. 3. Effects of GTP40 intervention on the expression of lipid metabolism-related genes in the liver and adipose tissue of HFD-fed hyperlipidemic mice. Relative expression levels of (A) *Adipor1*, (B) *AMPKα*, (C) *SREBP-1c*, (D) *FAS*, (E) *ACCα*, (F) *PPARα*, and (G) *CPT-1α* in liver; Relative expression levels of *UCP1* in (H) sWAT and (I) BAT. Data were expressed as m ± SD (n = 4). Data with different letters varied significantly ($p < 0.05$). Adipor1, adiponectin receptor 1; AMPKα, AMP-activated protein kinase alpha; SREBP-1c, Sterol regulatory element-binding protein 1c; FAS, fatty acid synthase; ACCα, acetyl-CoA carboxylase alpha; PPARα, peroxisome proliferator-activated receptor alpha; CPT-1α, carnitine palmitoyl transferase 1 alpha; UCP1, uncoupling protein 1; sWAT, subcutaneous inguinal white adipose tissues; BAT, brown adipose tissue.

Table 1
The yields and physiochemical properties of GTP40–1P, GTP40–3P, and GTP40–5P.

	GTP40–1P	GTP40–3P	GTP40–5P
Yield/%	~26.30	~24.85	~17.55
Neutral sugar/%	28.30 ± 0.31	49.90 ± 0.31	62.30 ± 0.70
Protein/%	6.00 ± 1.08	4.38 ± 0.98	2.52 ± 0.74
Uronic acid/%	33.62 ± 3.50	43.20 ± 0.53	54.82 ± 0.51
M_w (Da)	94244	83256	27858
M_n (Da)	60437	53873	19516
M_w/M_n	1.559	1.545	1.427

3.5.2. 1D/2D NMR analysis

^{1}H NMR is used to determine the type, configuration, and relative content of sugar residues. The number of peaks in the anomeric proton region reflects the number of monosaccharide residue types, and the relative ratio of each monosaccharide residue can be roughly estimated based on the peak area. A chemical shift of anomeric proton greater than 5.0 ppm indicated an *α*-type configuration, whereas a signal less than 5.0 ppm implied a *β*-type (Yuan et al., 2016). However, due to the influence of the carbon atoms, the proton signals of H_2~H_6 were severely overlapped in the chemical shift range of 3.0–5.5 ppm, but could be well separated in the COSY spectra. In Fig. 6A, four major peaks were identified at δ 5.01, 4.88, 4.56 and 4.38 ppm in the ^{1}H NMR spectrum, which were labelled as **Residue A**, **B**, **C**, and **D**, respectively. The high-intensity peak around δ 4.70 ppm was attributed to the presence of D_2O. As presented in Fig. 6B, the carbon signals in the ^{13}C NMR spectrum were mainly distributed between δ 60–120 ppm, with a characteristic peak at δ 172.12 ppm corresponding to the C_6 signal from uronic acids (Hong et al., 2022). The signal around δ 54.20 ppm was assigned to the methyl carbon group of methylated galacturonic acid (Li et al., 2014).

In the HSQC spectrum (Fig. 6D), a strong cross peak of the anomeric carbon signal (C_1) at δ 101.77 ppm and its corresponding anomeric proton signal (H_1) at δ 4.88 ppm were observed. In the COSY spectrum (Fig. 6C), cross peaks were found at H_1/H_2 (4.88/3.67), H_2/H_3 (3.67/3.93), H_3/H_4 (3.93/4.38), H_4/H_5 (4.38/5.05). Therefore, it was inferred that H_1, H_2, H_3, H_4, and H_5 were assigned to δ 4.88, 3.67, 3.93, 4.38, and

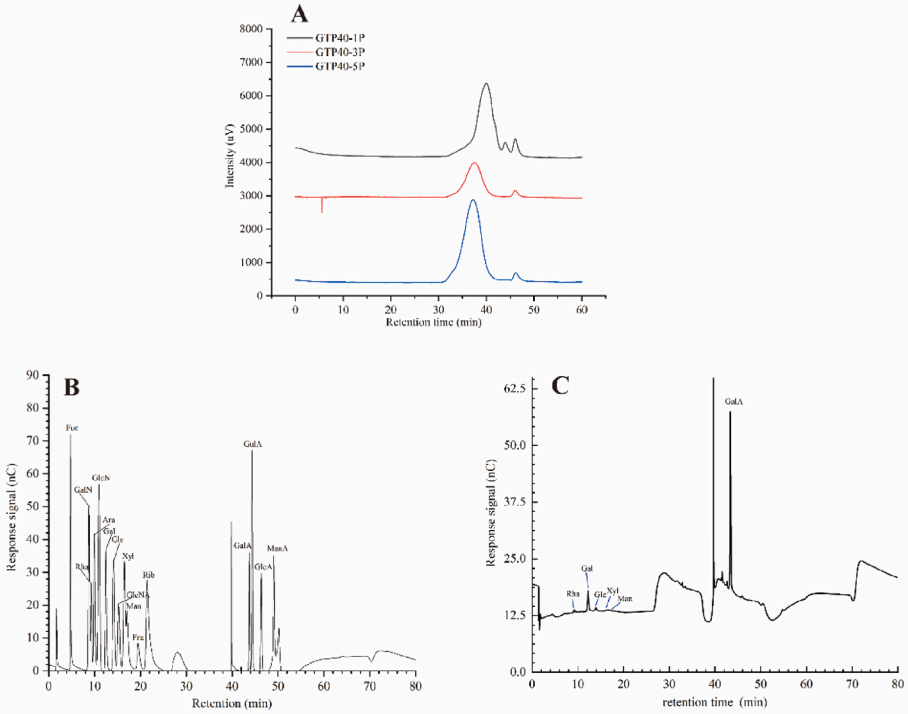

Fig. 4. The HPGPC chromatogram of GTP40–1P, GTP40–3P, and GTP40–5P (A), ion chromatogram of 16 mixed standards (B) and GTP40–5P (C). GTP40–1P, GTP40–3P, GTP40–5P represent the degradation products of GTP40 treated with TFA for 1, 3, 5 h, respectively.

Table 2
Methylation analysis of GTP40–5P.

Retention time (min)	PMAAs[a]	Mass fragments (m/z)	Relative molar ratio[b] (%)	Linkage pattern
24.833	2,3,4,6-Me_4-Gal*p*	43,71,87,101,117,129,145,161,205	7.60	t-Gal*p*1→
29.040	2,3,6-Me_3-Gal*p*	43,71,87,99,101,113,117,129,131,161,173,233	80.06	→4-Gal*p*1→
33.338	2,6-Me_2-Gal*p*	43,87,97,117,129,143,159,185	12.34	→3,4-Gal*p*1→

[a] Partially methylated alditol acetate.
[b] Calculated according to the ratio of peak areas.

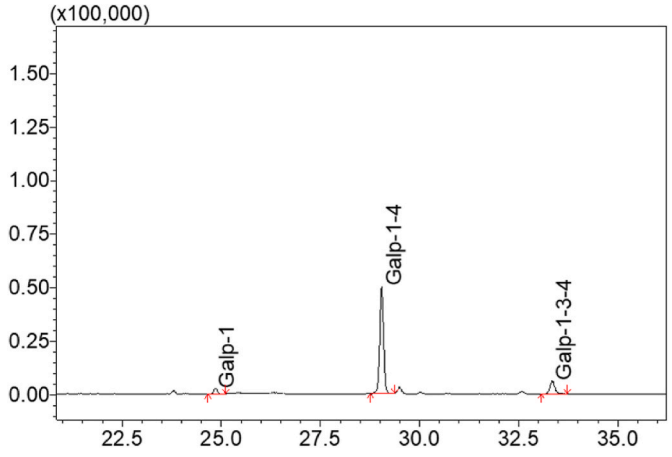

Fig. 5. Gas chromatogram of PMAAs derived from GTP40–5P.

5.05 ppm, respectively. Their corresponding carbon signals of C_1~C_5 were determined to be 101.77, 69.40, 70.05, 79.15, and 72.65 ppm in the HMBC spectrum (Fig. 6E). However, the signal of C6 was at δ 172.12 ppm, and an intense cross peak was observed at 3.73/54.20 ppm in the HSQC spectrum (Fig. 6D), which belonged to the proton and carbon signals of the methoxy group (Ghosh et al., 2009; Li et al., 2014), suggesting that **Residue B** was identified as →4)-*α*-D-Gal*p*A-(1→, with partial methyl esterification of some carboxyl groups. **Residues C** and **D** were identified in the same manner.

HMBC and NOESY spectra were applied to identify the linkage sites and sequence of neighbouring sugar residues (Fig. 6F–G). Evidently, in the NOESY spectrum, a cross peak of H_1/H_4 (**Residue B**, δ 4.88 ppm/**Residue B**, δ 4.88 ppm) was observed, suggesting the existence of →4)-*α*-D-Gal*p*A-(1 → 4)-*α*-D-Gal*p*A-(1 → . A cross peak of H_1/H_4 (**Residue B**, δ 4.88 ppm/**Residue A**, δ 4.39 ppm) indicated the presence of →4)-*α*-D-Gal*p*A-(1 → 3,4)-*α*-D-Gal*p*A-(1 → . Additionally, the cross peak of H_1/H_4 (**Residue A**, δ 5.01 ppm/**Residue C**, δ 4.08 ppm) demonstrated the presence of →3,4)-*α*-D-Gal*p*A-(1 → 4)-*β*-D-Galp-(1 → . The cross peak of H_1/H_3 (**Residue D**, δ 4.38 ppm/**Residue A**, δ 4.09 ppm) indicated the presence of *β*-D-Gal*p*-(1 → 3,4)-*α*-D-Gal*p*A-(1 → . Combining all the information from ^1H, ^{13}C, COSY, HSQC and HMBC spectra, the complete assignments of each residue were listed in Table 3. Therefore, it was inferred that the backbone of GTP40–5P was composed of →4)-*α*-D-Gal*p*A-(1 → 4)-*β*-D-Gal*p*-(1→ with partial methyl esterification, and the terminal residue *β*-D-Gal*p*-(1→ was linked to →3,4)-*α*-D-Gal*p*A-(1→ at the *O*-3 site. In conclusion, the possible repeating unit structure of GTP40–5P was elucidated as follows.

4. Conclusion

In this study, the effect of GTP40 on lipid metabolism in hypoglycemic mice induced by HFD, as well as its structural characteristics were

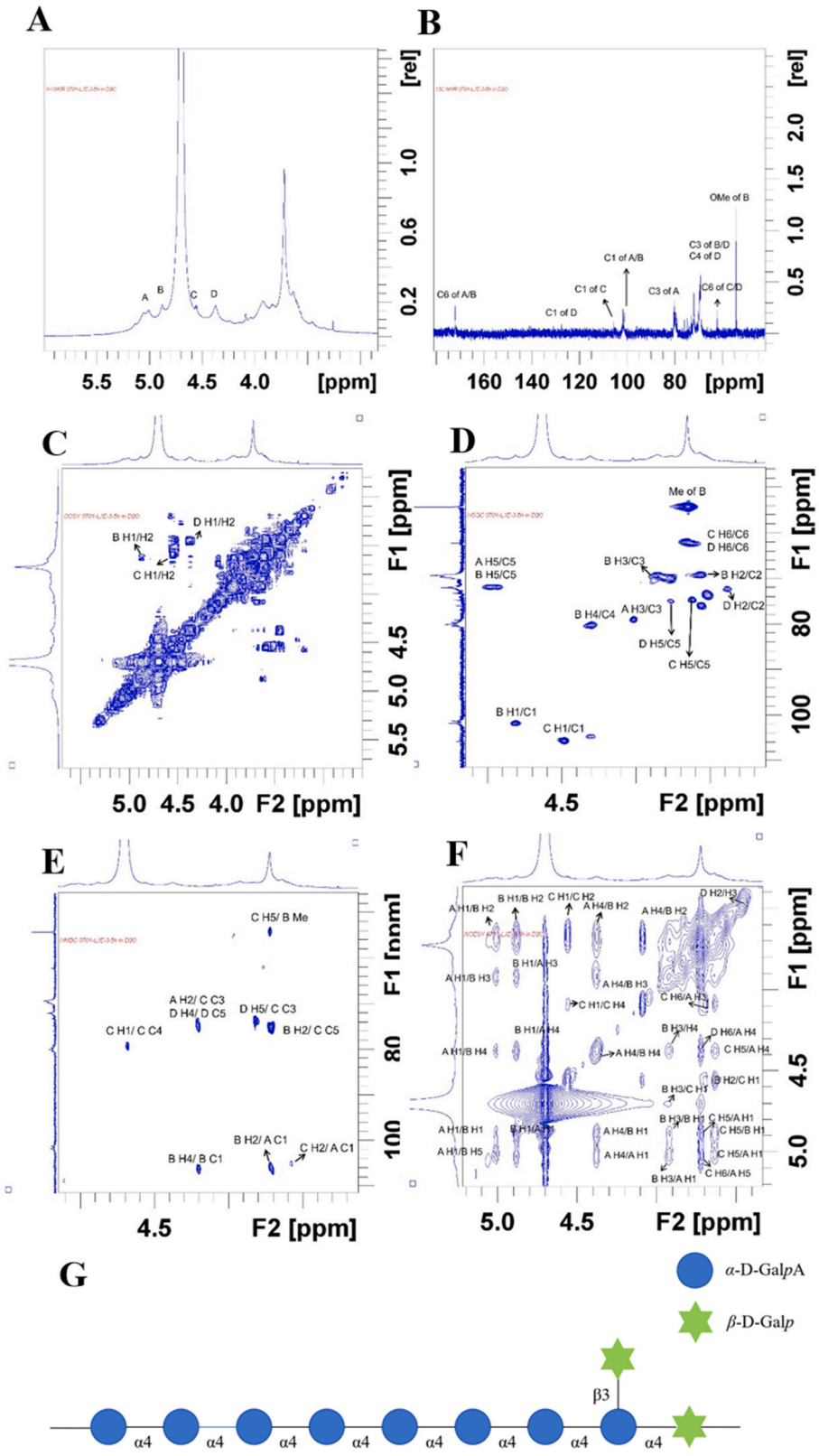

Fig. 6. 1D/2D NMR spectra of GTP40–5P. (A) ^{1}H NMR spectrum, (B) ^{13}C NMR spectrum, (C) COSY spectrum, (D) HSQC spectrum, (E) HMBC spectrum, (F) NOESY spectrum, and (G) inferred chain structure of GTP40–5P. GTP40–5P represents the degradation product of GTP40 treated with TFA for 5 h.

investigated. GTP40 significantly reduced the indices of the various adipose tissues, and decreased the size of adipocytes in a dose-dependent manner. Oxidative stress in the liver was also significantly ameliorated after GTP40 treatment. RT-qPCR results showed that GTP40 treatment upregulated genes related to lipolysis (*AMPKα*, *PPARα*, and *CPT-1α*) and downregulated genes related to adipogenesis (*SREBP-1c*, *ACCα*, and *FAS*). The results indicated that the regulatory mechanism of GTP40 on lipid metabolism likely involves activating

Table 3
Chemical shifts (δ) of ^{1}H NMR and ^{13}C NMR spectra of GTP40–5P.

Glycosyl residues	H1/C1	H2/C2	H3/C3	H4/C4	H5/C5	H6/C6	O-CH_3
A →3,4)-α-D-GalpA-(1→	5.01 101.34	4.17 72.70	4.09 82.55	4.39 79.15	5.07 71.83	 172.12	
B →4)-α-D-GalpA6Me-(1→	4.88 101.77	3.67 69.40	3.93 70.05	4.38 79.15	5.05 72.65	 172.12	3.73 54.20
C →4)-β-D-Galp-(1→	4.56 105.80	3.60 73.21	3.69 74.84	4.08 79.03	3.63 76.01	3.72 62.10	
D β-D-Galp-(1→	4.38 108.18	3.45 72.10	4.04 70.56	4.26 71.35	3.83 74.5	3.71 62.11	

AMPK signaling pathway to enhance fatty acid oxidation and inhibit fat production, as well as activating BAT to induce non-shivering thermogenesis. Three acid hydrolysis products, namely GTP40–1P, GTP40–3P, and GTP40–5P were obtained by the partial acid hydrolysis method, and their chemical compositions were determined. GTP40–5P exhibited increased contents of neutral sugar, uronic acid, and protein, with a minimum M_w/M_n value, suggesting the most uniform molecular weight distribution. The backbone of GTP40–5P consisted of →4)-α-D-Gal*p*A-(1 → 4)-β-D-Gal*p*-(1→, and the terminal residue β-D-Gal*p*-(1→ was linked to →3,4)-α-D-GalA*p*-(1→ at the *O*-3 site. These results contribute to revealing the structure-activity relationship of Gougunao tea polysaccharide and provide a theoretical basis for its application in the food and pharmaceutical industries. In addition, further investigations into appetite regulation, gut microbiota composition, metabolomics profiling, and other related factors, along with correlation analyses, would provide deeper insights into the lipid-lowering mechanisms of Gougunao tea polysaccharide.

CRediT authorship contribution statement

Qihuan Deng: Data curation, Formal analysis, Investigation, Methodology, Software, Writing – original draft. **Shiyi Xiong:** Data curation, Formal analysis, Methodology, Software, Writing – original draft, Writing – review & editing. **Wenjun Wang:** Writing – review & editing. **Guodong Zheng:** Formal analysis, Supervision, Writing – review & editing. **Jingjing Xie:** Software, Validation. **Xiaojin He:** Software, Validation. **Liang Ye:** Software, Validation. **Lili Yu:** Formal analysis, Investigation. **Jingen Li:** Funding acquisition, Project administration, Resources, Supervision, Validation, Writing – review & editing.

Declaration of competing interest

The authors declare that they have no known financial interests or personal relationships that might influence the work reported here.

Acknowledgements

Financial support from Jiangxi Provincial Natural Science Foundation (20224BAB205044), Undergraduate Innovation and Entrepreneurship Training Project (202410410204), and the open project program of State Key Laboratory of Food Science and Resources, Nanchang University (SKLF-KF-202410).

Appendix A. Supplementary data

Supplementary data to this article can be found online at https://doi.org/10.1016/j.crfs.2025.101103.

Data availability

The data that has been used is confidential.

References

Auclair, M., Roblot, N., Capel, E., Fève, B., Antoine, B., 2020. Pharmacological modulation of RORα controls the fat browning, adaptive thermogenesis and body weight in mice. Am. J. Physiol. Endocrimol. Metab. 320 (2), 219–233. https://doi.org/10.1152/ajpendo.00131.2020.

Bian, Y., Li, X., Li, X., Ju, J.M., Liang, H.F., Hu, X.L., Dong, L., Wang, N., Li, J.M., Zhang, Y., Yang, B.F., 2019. Daming capsule, a hypolipidaemic drug, lowers blood lipids by activating the AMPK signalling pathway. Biomed. Pharmacother. 117, 109176. https://doi.org/10.1016/j.biopha.2019.109176.

Bradford, M.M., 1976. A rapid and sensitive method for the quantitation of microgram quantities of protein utilizing the principle of protein-dye binding. Anal. Biochem. 72, 248–254. https://doi.org/10.1016/0003-2697(76)90527-3.

Broadfield, L.A., Pane, A.A., Talebi, A., Swinnen, J.V., Fendt, S.M., 2021. Lipid metabolism in cancer: new perspectives and emerging mechanisms. Dev. Cell 56 (10), 1363–1393. https://doi.org/10.1016/j.devcel.2021.04.013.

Chao, C.Y., Huang, C.J., 2020. *In vitro* activation of peroxisome proliferator activated receptor α by some extracts from food materials. J. Food Drug Anal. 16, 62–69. https://doi.org/10.38212/2224-6614.2342.

Chen, L., Wang, Y.X., Liu, J.X., Hong, Z.Y., Wong, K.H., Chiou, J.C., Xu, B.J., Cespedes-Acuña, C.L., Bai, W.B., Tian, L.M., 2023. Structural characteristics and *in vitro* fermentation patterns of polysaccharides from *Boletus* mushrooms. Food Funct. 14, 7912–7923. https://doi.org/10.1039/D3FO01085F.

Deng, Q.H., Wang, W.J., Zhang, L.Y., Chen, L.L., Zhang, Q.F., Zhang, Y., He, S.C., Li, J.E., 2023. Gougunao tea polysaccharides ameliorate high-fat diet-induced hyperlipidemia and modulate gut microbiota. Food Funct. 14, 703–719. https://doi.org/10.1039/D2FO01828D.

Deng, Q.H., Wang, W.J., Zhang, Q.F., Chen, J.G., Zhou, H., Meng, W.Y., Li, J.E., 2021. Extraction optimization of polysaccharides from Gougunao tea and assessment of the antioxidant and hypoglycemic activities of its fractions *in vitro*. Bioact. Carbohydr. Diet. Fibre 26, 100287. https://doi.org/10.1016/j.bcdf.2021.100287.

Dong, J.J., Wang, W.J., Zheng, G.D., Wu, N.S., Xie, J.J., Xiong, S.Y., Tian, P.T., Li, J.E., 2024. *In vitro* digestion and fermentation behaviors of polysaccharides from *Choerospondias axillaris* fruit and its effect on human gut microbiota. Curr. Res. Food Sci. 8, 100760. https://doi.org/10.1016/j.crfs.2024.100760.

Du, L.L., Fu, Q.Y., Xiang, L.P., Zheng, X.Q., Lu, J.L., Ye, J.H., Li, Q.S., Polito, C., Liang, Y. R., 2016. Tea polysaccharides and their bioactivities. Molecules (Basel) 21 (11), 1449. https://doi.org/10.3390/molecules21111449.

Duan, Y.Q., Hu, Z.Y., Jin, L., Zong, T.Q., Zhang, X.H., Liu, Y.N., Yang, P.C., Sun, J.F., Zhou, W., Li, G., 2024. Efficient degradation and enhanced anticomplementary activity of *Belamcanda chinensis (L.) DC.* polysaccharides via trifluoroacetic acid treatment with different degrees. Int. J. Biol. Macromol. 276, 134117. https://doi.org/10.1016/j.ijbiomac.2024.134117.

Fan, Z.X., Chen, X.J., Liu, T.Z., Yu, Q.H., Song, Z.Q., Wang, F., Li, T.P., 2022. Pectin oligosaccharides improved lipid metabolism in white adipose tissue of high-fat diet fed mice. Food Sci. Biotechnol. 31, 1197–1205. https://doi.org/10.1007/s10068-022-01109-9.

Ghosh, K., Chandra, K., Ojha, A.K., Sarkar, S., Islam, S.S., 2009. Structural identification and cytotoxic activity of a polysaccharide from the fruits of *Lagenaria siceraria* (Lau). Carbohydr. Res. 344, 693–698. https://doi.org/10.1016/j.carres.2009.01.012.

Gloaguen, V., Plancke, Y., Strecker, G., Vebret, L., Hoffmann, L., Morvan, H., 1997. Structural characterization of three aldobiuronic acids derived from the capsular polysaccharide produced by the thermophilic cyanobacterium Mastigocladus laminosus. Int. J. Biol. Macromol. 21, 73–79. https://doi.org/10.1016/S0141-8130(97)00044-5.

Han, H.J., Song, X.J., Yadav, D., Hwang, M.S., Lee, J.H., Lee, C.H., Kim, T.H., Lee, J.J., Kwon, J., 2019. Ulmus macrocarpa Hance modulates lipid metabolism in hyperlipidemia *via* activation of AMPK pathway. PLoS One 14 (5), e0217112. https://doi.org/10.1371/journal.pone.0217112.

Hegazy, M., El-Shafey, M., Abulsoud, A.I., Elsadek, B.E.M., Abd Elaziz, A.I., Salama, S.A., 2020. Pioglitazone ameliorates high fat diet-induced hypertension and induces catechol o-methyl transferase expression in rats. Eur. J. Pharmacol. 885, 173383. https://doi.org/10.1016/j.ejphar.2020.173383.

Heidary Moghaddam, R., Samimi, Z., Asgary, S., Mohammadi, P., Hozeifi, S., Hoseinzadeh-Chahkandak, F., Xu, S., Farzaei, M.H., 2022. Natural AMPK activators in cardiovascular disease prevention. Front. Pharmacol. 12, 738420. https://doi.org/10.3389/fphar.2021.738420.

Hong, T., Zhao, J.Y., Yin, J.Y., Nie, S.P., Xie, M.Y., 2022. Structural characterization of a low molecular weight HG-type pectin from Gougunao Green Tea. Front. Nutr. 9, 878249. https://doi.org/10.3389/fnut.2022.878249.

Hung, C.M., Calejman, C.M., Sanchez-Gurmaches, J., Li, H., Clish, C.B., Hettmer, S., Wagers, A.J., Guertin, D.A., 2014. Rictor/mTORC2 Loss in the Myf5 lineage reprograms brown fat metabolism and protects mice against obesity and metabolic disease. Cell Rep. 8, 256–271. https://doi.org/10.1016/j.celrep.2014.06.007.

Jin, W.H., Wang, J., Ren, S.M., Song, N., Zhang, Q.B., 2012. Structural analysis of a heteropolysaccharide from *Saccharina japonica* by electrospray mass spectrometry in tandem with collision-induced dissociation tandem mass spectrometry (ESI-CID-MS/MS). Mar. Drugs 10, 2138–2152. https://doi.org/10.3390/md10102138.

Ju, M.Z., Liu, Y.Q., Li, M.Y., Cheng, M.J., Zhang, Y., Deng, G.Z., Kang, X.J., Liu, H., 2019. Baicalin improves intestinal microecology and abnormal metabolism induced by high-fat diet. Eur. J. Pharmacol. 857, 172457. https://doi.org/10.1016/j.ejphar.2019.172457.

Kang, J., Cui, S.W., Guo, Q.B., Chen, J., Wang, Q., Phillips, G.O., Nikiforuk, J., 2012. Structural investigation of a glycoprotein from gum ghatti. Carbohydr. Polym. 89, 749. https://doi.org/10.1016/j.carbpol.2012.04.004, 758.

Kang, J.H., Kim, H.S., Park, S.H., Kim, Y.S., Bae, S., 2023. WKYMVm ameliorates obesity by improving lipid metabolism and leptin signalling. J. Cell Mol. Med. 27 (18), 2782–2791. https://doi.org/10.1111/jcmm.17910.

Karise, I., Bargut, T.C., Del Sol, M., Aguila, M.B., Mandarim-de-Lacerda, C.A., 2019. Metformin enhances mitochondrial biogenesis and thermogenesis in brown adipocytes of mice. Biomed. Pharmacother. 111, 1156–1165. https://doi.org/10.1016/j.biopha.2019.01.021.

Kim, M.R., Kim, J.W., Park, J.B., Hong, Y.K., Ku, S.K., Choi, J.S., 2017. Anti-obesity effects of yellow catfish protein hydrolysate on mice fed a 45% kcal high-fat diet. Int. J. Mol. Med. 40, 784–800. https://doi.org/10.3892/ijmm.2017.3063.

Lan, Y., Sun, Q.Y., Ma, Z.Y., Peng, J., Zhang, M.Q., Wang, C., Zhang, X.T., Yan, X.F., Chang, L.L., Hou, X.L., Qiao, R.X., Mulati, A., Zhou, Y., Zhang, Q., Liu, Z.G., Liu, X.B., 2022. *Seabuckthorn* polysaccharide ameliorates high-fat diet-induced obesity by gut microbiota-SCFAs-liver axis. Food Funct. 13, 2925–2937. https://doi.org/10.1039/D1FO03147C.

Li, J.E., Deng, Q.H., Yu, X.Y., Wang, W.J., 2020. Structural studies of a new fraction obtained by gradient ethanol precipitation from *Acacia seyal* gum. Food Hydrocoll. 107, 105932. https://doi.org/10.1016/j.foodhyd.2020.105932.

Li, J.E., Cui, S.W., Nie, S.P., Xie, M.Y., 2014. Structure and biological activities of a pectic polysaccharide from *Mosla chinensis Maxim. cv. Jiangxiangru*. Carbohydr. Polym. 105, 276–284. https://doi.org/10.1016/j.carbpol.2014.01.081.

Li, Z., Yi, C.X., Katiraei, S., Kooijman, S., Zhou, E., Chung, C.K., Gao, Y., Van Den Heuvel, J.K., Meijer, O.C., Berbée, J.F.P., Heijink, M., Giera, M., Willems Van Dijk, K., Groen, A.K., Rensen, P.C.N., Wang, Y., 2018. Butyrate reduces appetite and activates brown adipose tissue via the gut-brain neural circuit. Gut 67, 1269–1279. https://doi.org/10.1136/gutjnl-2017-314050.

Lu, P., Zhang, F.C., Qian, S.W., Li, X., Cui, Z.M., Dang, Y.J., Tang, Q.Q., 2016. Artemisinin derivatives prevent obesity by inducing browning of WAT and enhancing BAT function. Cell Res. 26, 1169–1172. https://doi.org/10.1038/cr.2016.108.

Ma, C.L., Bai, J.W., Shao, C.T., Liu, J.W., Zhang, Y., Li, X.Q., Yang, Y., Xu, Y.Q., Wang, L. B., 2021. Degradation of blue honeysuckle polysaccharides, structural characteristics and antiglycation and hypoglycemic activities of degraded products. Food Res. Int. 143, 110281. https://doi.org/10.1016/j.foodres.2021.110281.

Okada-Iwabu, M., Yamauchi, T., Iwabu, M., Honma, T., Hamagami, K., Matsuda, K., Yamaguchi, M., Tanabe, H., Kimura-Someya, T., Shirouzu, M., Ogata, H., Tokuyama, K., Ueki, K., Nagano, T., Tanaka, A., Yokoyama, S., Kadowaki, T., 2013. A small-molecule AdipoR agonist for type 2 diabetes and short life in obesity. Nature 503 (7477), 493–499. https://doi.org/10.1038/nature12656.

Pan, Y.Y., Zeng, F., Guo, W.L., Li, T.T., Jia, R.B., Huang, Z.R., Lv, X.C., Zhang, J., Liu, B., 2018. Effect of *Grifola frondosa* 95% ethanol extract on lipid metabolism and gut microbiota composition in high-fat diet-fed rats. Food Funct. 9, 6268–6278. https://doi.org/10.1039/C8FO01116H.

Pandeirada, C.O., Speranza, S., Bakx, E., Westphal, Y., Janssen, H.G., Schols, H.A., 2022. Partial acid-hydrolysis of TEMPO-oxidized arabinoxylans generates arabinoxylan-structure resembling oligosaccharides. Carbohydr. Polym. 276, 118795. https://doi.org/10.1016/j.carbpol.2021.118795.

Perez-Luz, S., Matamala, N., Gomez-Mariano, G., Janciauskiene, S., Martínez-Delgado, B., 2023. NAFLD and AATD are two diseases with unbalanced lipid metabolism: similarities and differences. Biomedicines 11 (7), 1961. https://doi.org/10.3390/biomedicines11071961.

Qiu, J.Q., Zhang, H., Wang, Z.Y., 2019. Ultrasonic degradation of polysaccharides from *Auricularia auricula* and the antioxidant activity of their degradation products. LWT 113, 108266. https://doi.org/10.1016/j.lwt.2019.108266.

Qiu, S.Q., Huang, L., Xia, N., Teng, J.W., Wei, B.Y., Lin, X.S., Khan, M.R., 2022. Two polysaccharides from Liupao Tea exert beneficial effects in simulated digestion and fermentation model *in vitro*. Foods 11, 2958. https://doi.org/10.3390/foods11192958.

Rudtanatip, T., Pariwatthanakun, C., Somintara, S., Sakaew, W., Wongprasert, K., 2022. Structural characterization, antioxidant activity, and protective effect against hydrogen peroxide-induced oxidative stress of chemically degraded *Gracilaria fisheri* sulfated galactans. Int. J. Biol. Macromol. 206, 51–63. https://doi.org/10.1016/j.ijbiomac.2022.02.125.

Wang, Q.H., Tang, J., Jiang, S.J., Huang, Z., Song, A.Y., Hou, S.Y., Gao, X., Ruan, H.B., 2018. Inhibition of PPARγ, adipogenesis and insulin sensitivity by MAGED1. J. Endocrinol. 239, 167–180. https://doi.org/10.1530/JOE-18-0349.

Xiong, F., Li, X., Zheng, L.H., Hu, N., Cui, M.J., Li, H.Y., 2019. Characterization and antioxidant activities of polysaccharides from *Passiflora edulis Sims peel* under different degradation methods. Carbohydr. Polym. 218, 46–52. https://doi.org/10.1016/j.carbpol.2019.04.069.

Xu, Z., Huang, J.C., Wen, M., Zhang, X.T., Lyu, D.X., Li, S.S., Xiao, H.M., Li, M., Shen, C. P., Huang, H.Q., 2024. Gentiopicroside ameliorates glucose and lipid metabolism in T2DM *via* targeting FGFR1. Phytomedicine (Stuttg.) 132, 155780. https://doi.org/10.1016/j.phymed.2024.155780.

Yang, M., Yin, Y.X., Wang, F., Zhang, H.H., Ma, X.K., Yin, Y.L., Tan, B., Chen, J.S., 2021. Supplementation with *Lycium barbarum* polysaccharides reduce obesity in high-fat diet-fed mice by modulation of gut microbiota. Front. Microbiol. 12, 719967. https://doi.org/10.3389/fmicb.2021.719967.

Yang, Y.J., Yin, X.X., Zhang, D.J., Zhang, B.Y., Lu, J., Wang, X.H., 2022. Structural characteristics, antioxidant, and immunostimulatory activities of an acidic polysaccharide from *Raspberry Pulp*. Molecules (Basel) 27, 4385. https://doi.org/10.3390/molecules27144385.

Yuan, D., Huang, Q., Li, C., Fu, X., 2022. A polysaccharide from *Sargassum pallidum* reduces obesity in high-fat diet-induced obese mice by modulating glycolipid metabolism. Food Funct. 13, 7181–7191. https://doi.org/10.1039/D2FO00890D.

Yuan, Y.F., Wang, Y.B., Jiang, Y.M., Prasad, K.N., Yang, J.L., Qu, H.X., Wang, Y., Jia, Y. X., Mo, H., Yang, B., 2016. Structure identification of a polysaccharide purified from *Lycium barbarium* fruit. Int. J. Biol. Macromol. 82, 696–701. https://doi.org/10.1016/j.ijbiomac.2015.10.069.

Zhang, W.K., Yu, L.H., Yang, Q.R., Zhang, J.F., Wang, W.J., Hu, X.R., Li, J.E., Zheng, G. D., 2024. *Smilax China L.* polysaccharide prevents HFD induced-NAFLD by regulating hepatic fat metabolism and gut microbiota. Phytomedicine (Stuttg.) 127, 155478. https://doi.org/10.1016/j.phymed.2024.155478.

Zhu, Z.J., Zhu, B.W., Sun, Y.J., Ai, C.Q., Wang, L.L., Wen, C.R., Yang, J.F., Song, S., Liu, X.L., 2018. Sulfated polysaccharide from *Sea Cucumber* and its depolymerized derivative prevent obesity in association with modification of gut microbiota in high-fat diet-fed mice. Mol. Nutr. Food Res. 62, 1800446. https://doi.org/10.1002/mnfr.201800446.